BIOCHEMISTRY
including biophysical chemistry & molecular biology
Article

Biochemistry **2009,** *48,* 5953–5962 5953
DOI: 10.1021/bi900426d

Probing Protein Folding Using Site-Specifically Encoded Unnatural Amino Acids as FRET Donors with Tryptophan†

Shigeki J. Miyake-Stoner, Andrew M. Miller, Jared T. Hammill, Jennifer C. Peeler, Kenneth R. Hess, Ryan A. Mehl,* and Scott H. Brewer*

Department of Chemistry, Franklin & Marshall College, Lancaster, Pennsylvania 17604-3003

Received March 11, 2009; Revised Manuscript Received May 7, 2009

ABSTRACT: The experimental study of protein folding is enhanced by the use of nonintrusive probes that are sensitive to local conformational changes in the protein structure. Here, we report the selection of an aminoacyl-tRNA synthetase/tRNA pair for the cotranslational, site-specific incorporation of two unnatural amino acids that can function as fluorescence resonance energy transfer (FRET) donors with Trp to probe the disruption of the hydrophobic core upon protein unfolding. L-4-Cyanophenylalanine (pCNPhe) and 4-ethynylphenylalanine (pENPhe) were incorporated into the hydrophobic core of the 171-residue protein, T4 lysozyme. The FRET donor ability of pCNPhe and pENPhe is evident by the overlap of the emission spectra of pCNPhe and pENPhe with the absorbance spectrum of Trp. The incorporation of both unnatural amino acids in place of a phenylalanine in the hydrophobic core of T4 lysozyme was well tolerated by the protein, due in part to the small size of the cyano and ethynyl groups. The hydrophobic nature of the ethynyl group of pENPhe suggests that this unnatural amino acid is a more conservative substitution into the hydrophobic core of the protein compared to pCNPhe. The urea-induced disruption of the hydrophobic core of the protein was probed by the change in FRET efficiency between either pCNPhe or pENPhe and the Trp residues in T4 lysozyme. The methodology for the study of protein conformational changes using FRET presented here is of general applicability to the study of protein structural changes, since the incorporation of the unnatural amino acids is not inherently limited by the size of the protein.

The study of protein folding and unfolding is an active area of research both experimentally and computationally due in part to the connection between protein misfolding and numerous disease states (*1*−*6*). The experimental study of protein folding has utilized a number of spectroscopic techniques, including IR, Raman, NMR, CD, DSC, and fluorescence spectroscopy to probe peptide−backbone conformational changes associated with protein folding (*7*−*14*). Several of these spectroscopic techniques have been coupled with specific labels for exploring local conformational changes in proteins to obtain a more detailed view of protein structure and folding. For instance, IR spectroscopy has been used in conjunction with $^{13}C{=}^{16}O$ and $^{13}C{=}^{18}O$ isotopic labels in the peptide backbone of specific residues to monitor local changes in the backbone conformation (*15*−*22*). Fluorescence spectroscopy has been used in conjunction with a number of fluorophores, such as Trp, to probe local conformational changes in proteins, since Trp emission is sensitive to changes in its local environment (*12*, *23*−*25*). Protein folding or unfolding has also been monitored by properly positioned fluorescence resonance energy transfer (FRET) pairs to probe the distance between the donor and acceptor of the FRET pair (*13*, *14*, *26*−*31*).

Recently, a new FRET pair consisting of the unnatural amino acid L-4-cyanophenylalanine (pCNPhe) as the donor molecule and the amino acid Trp as the acceptor molecule has been utilized to probe peptide conformational changes (*13*, *14*, *29*−*31*). These changes were monitored by measuring the observed fluorescence of pCNPhe as a function of peptide structure, since the efficiency of resonance energy transfer is dependent upon the distance between the donor and acceptor. Specifically, an increase in the observed emission of the donor suggests an increase in the distance between the donor and acceptor, which is modulated by peptide conformational changes.

Site-specific genetic incorporation of unnatural amino acids (UAAs) has expanded the scope of spectroscopic studies on large proteins, since defined spectroscopic labels can be incorporated into proteins *in vivo* (*32*−*36*). The unnnatural amino acid, pCNPhe, has previously been site-specifically incorporated into proteins via an evolved aminoacyl-tRNA synthetase; while it has been shown to function as an IR probe, its use as a FRET pair in proteins has not been explored (*37*). Similar methods have incorporated alkyne-containing UAAs into proteins for use as sites of chemical conjugation (*38*−*40*). None of these

†This work was supported by F&M Hackman and Eyler funds, NSF-MCB-0448297, Research Corporation (CC6364), Research Corporation (CC7352), and ACS-PRF (42214-GB4).

*To whom correspondence should be addressed. R.A.M.: e-mail, ryan.mehl@fandm.edu; phone, 717-291-4125; fax, 717-291-4343. S.H.B.: e-mail, scott.brewer@fandm.edu; phone, 717-358-4766; fax, 717-291-4343.

Published on Web 06/03/2009

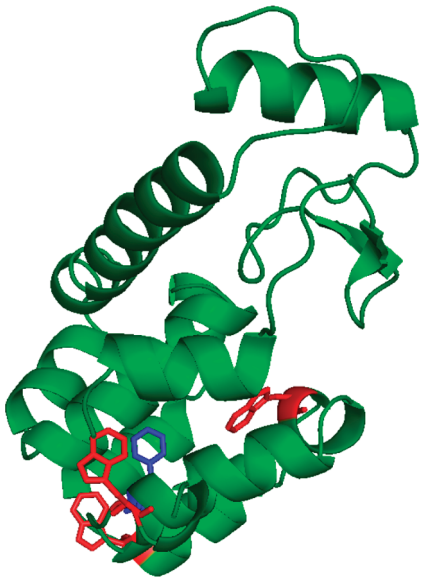

FIGURE 1: Structure of T4 lysozyme (PDB ID 1L63) highlighting phenylalanine residue 153 (blue) that has been replaced selectively with either pCNPhe or pENPhe to act as FRET donors with the Trp acceptors (Trp126, Trp138, Trp158) shown in red.

alkynyl-UAAs, however, have the extended conjugation needed to function as a FRET pair with Trp.

Here we report the evolution and characterization of an aminoacyl-tRNA synthetase/tRNA pair for the cotranslational, site-specific incorporation of both pCNPhe and the novel 4-ethynylphenylalanine (pENPhe). We have investigated the ability of both the pCNPhe and Trp FRET pair and the pENPhe and Trp FRET pair to probe the protein conformational changes resulting from the urea-induced unfolding of the well-studied protein, T4 lysozyme (Figure 1) (*41*−*43*). Specifically, phenylalanine residue 153, located in the hydrophobic core of T4 lysozyme, was replaced with either pCNPhe or pENPhe. Figure 1 also shows the proximity of Phe153 with three Trp residues (W126, W138, and W158). The observed fluorescence of the donor molecule, either pCNPhe or pENPhe, in T4 lysozyme was measured as a function of concentration of the chemical denaturant, urea, used to modulate the structure of the protein. The resulting denaturation curves were fit to a two-state model of unfolding to determine the effectiveness of using these two unnatural amino acid FRET donors with Trp to probe local conformational changes in proteins.

EXPERIMENTAL PROCEDURES

General Methods. Chemical reagents were purchased from Sigma-Aldrich and Fisher Scientific and used without further purification. L-4-Cyanophenylalanine (pCNPhe) was purchased from Bachem. Racemic 4-ethynylphenylalanine (pENPhe) was synthesized based upon previous literature procedures (see Supporting Information) (*44*). Oligonucleotides, DH10B cells, and *pBadA* were purchased from Invitrogen.

Construction of Plasmids. *pDule-pspPhe* plasmid was generated by amplifying the aminoacyl-tRNA synthetase gene from the *pBK* plasmid isolated from the library using primers RS-move-F and RS-move-R. The amplified DNA fragments were cloned into a *pDule* plasmid using the incorporated *Nco*I and *Kpn*I sites (*45*). The *pBad-T4* plasmid was generated by using the WT*T4 gene from plasmid *pH1403* (*46*). Primers T4-move-F and T4-move-R were used to amplify the gene adding *Nco*I and *Sca*I cut and a C-terminal 6-His affinity purification tag, respectively. This new gene (T4-native) was subcloned into *pBadA*. The *pBad-T4-153TAG* plasmid was generated by QuikChange mutagenesis (Stratagene) on *pBad-T4* with primers T4-F153TAG-F and T4-F153TAG-R. After subcloning, all genes were confirmed by sequencing. See Supporting Information for a list of primers and genetic sequences.

Selection of p-spPhe Specific Aminoacyl-tRNA Synthetase (36, 47). The library of aminoacyl-tRNA synthetases was encoded on a kanamycin (Kn) resistant plasmid (*pBK*) under control of the constitutive *Escherichia coli* GlnRS promoter and terminator. The aminoacyl synthetase library (3D-Lib) was randomized as follows: Leu65, His70, Gln155, and Ile159 were randomized to all 20 natural amino acids; Tyr32 was randomized to 15 natural amino acids (less Trp, Phe, Tyr, Cys, and Ile); Asp158 was restricted to Gly, Ser, or Val; Leu162 was restricted to Lys, Ser, Leu, His, and Glu; and Phe108 and Gln109 were restricted to the pairs Trp-Met, Ala-Asp, Ser-Lys, Arg-Glu, Arg-Pro, Ser-His, or Phe-Gln (*48*). The library plasmid, *pBK-3D-Lib*, was moved between cells containing a positive selection plasmid (*pCG*) and cells containing a negative selection plasmid (*pNEG*) (*49*).

The positive selection plasmid, *pCG* (~10000 bp), encodes a mutant *Methanococcus jannaschii* (*Mj*) $tRNA^{Tyr}_{CUA}$, an amber codon disrupted chloramphenicol acetyltransferase, an amber codon disrupted T7 RNA polymerase that drives the production of green fluorescent protein, and the tetracycline (Tet) resistant marker. The negative selection plasmid, *pNEG* (~7000 bp), encodes the mutant $tRNA^{Tyr}_{CUA}$, an amber codon disrupted barnase gene under control of an arabinose promoter and rrnC terminator, and the ampicillin (Amp) resistant marker. *pCG* electrocompetent cells and *pNEG* electrocompetent cells were made from DH10B cells carrying the respective plasmids and stored in 100 μL aliquots at −80 °C for future rounds of selection.

The synthetase library in *pBK-3D-Lib* was transformed by electroporation into DH10B cells containing the Tet-resistant positive selection plasmid, *pCG*. The resulting *pCG*/*pBK-3D-Lib*-containing cells were amplified in 1 L of 2×YT with 50 μg/mL Kn and 25 μg/mL Tet with shaking at 37 °C. The cells were grown to saturation, then pelleted at 5525 rcf, resuspended in 30 mL of 2×YT and 7.5 mL of 80% glycerol, and stored at −80 °C in 1 mL aliquots for use in the first round of selections.

For the first positive selection, 1 mL of *pCG*/*pBK-3D-Lib* cells was thawed on ice before addition to 1 L of room temperature 2×YT media containing 50 μg/mL Kn and 25 μg/mL Tet. After incubation (14 h, 250 rpm, 37 °C), five 1 mL aliquots were pelleted (2000 rcf, 10 min) and resuspended in 2.5 mL of 2×YT media. A 250 μL aliquot of these cells was plated on ten 15 cm GMML-agar plates containing 50 μg/mL Kn, 25 μg/mL Tet, and 60 μg/mL chloramphenicol (Cm). The positive selection agar media also contained 1 mM pCNPhe. After spreading, the surface of the plates was allowed to dry completely before incubation (37 °C, 15 h). To harvest the surviving library members from the plates, 10 mL of 2×YT (50 μg/mL Kn, 25 μg/mL Tet) was added to each plate. Colonies were scraped from the plate using a glass spreader. The resulting solution was incubated (30 min, 37 °C) to wash cells free of agar. The cells were then pelleted, and plasmid DNA was extracted. For the first positive selection and first negative selection, a Qiagen midiprep kit was used to purify the plasmid DNA. For all other plasmid purification steps a Qiagen miniprep kit was used to purify the plasmid DNA. The smaller *pBK-3D-Lib* plasmid was separated

from the larger *pCG* plasmid by agarose gel electrophoresis and extracted from the gel using the Qiagen gel extraction kit.

For all subsequent positive selections, 2 μL (or ~50 ng) of purified library DNA was transformed into 100 μL of *pCG* competent cells. The transformants were rescued for 1.5 h in 1 mL of SOC (37 °C with shaking at 250 rpm), pelleted (1000 rcf for 5 min), and resuspended in 1 mL of LB media. A 50 μL sample of these cells was plated on three plates prepared as described in the first positive selection on LB agar plates, but the Cm concentration was raised to 80 μg/mL.

The purified *pBK-3D-Lib* was then transformed into *pNEG*-containing DH10B cells. A 100 μL sample of *pNEG* electrocompetent cells was transformed with 50 ng of purified *pBK-3D-Lib* DNA. Cells were rescued in 1 mL of SOC for 1 h (37 °C, 250 rpm). In the first negative selection, the entire 1 mL of rescue solution was plated on three 15 cm LB plates containing 100 μg/mL Amp, 50 μg/mL Kn, and 0.2% L-arabinose. In subsequent negative selections, one plate was spread with 250 μL of rescued cells, and two plates were spread with 50 mL of rescued cells and then incubated (12−16 h, 37 °C). Cells were collected from plates in the same manner as described above for positive selections. After a total of three rounds of positive and negative selection, remaining *pBK-3D-Lib* members were transformed into *pCG*-containing cells and grown on LB media plates in the presence of 1 mM pCNPhe, 60−80 μg/mL Cm, 50 μg/mL Kn, 25 μg/mL Tet, and 0.002% L-arabinose. Individual colonies (40) were selected from the surviving library and screened in the same media in the presence and absence of UAA with varying concentrations of Cm from 0 to 120 μg/mL. Individuals (10) showing the most growth in the Cm plates in the presence of pCNPhe and the least growth on Cm plates in the absence of pCNPhe were selected and sequenced.

Optimized Expression and Purification of T4 Lysozyme-Containing UAAs. All protein expressions were performed in DH10B cells transformed either with *pBad-T4* to produce wtT4 or with *pBad-T4-153TAG* and *pDule-pspPhe* to produce T4 that contains UAAs. The autolytic nature of T4 lysozyme prevented the use of standard autoinduction media methods to produce natural and UAA−protein constructs (*45*). For protein production, arabinose was withheld from the media. Cultures at 37 °C were inoculated with a 1:50 dilution of saturated cultures (OD ≥ 4.5). UAAs were dissolved in sterile water and 1 molar equiv of aqueous NaOH and then were added to the appropriate cultures when the cell densities reached an OD of 0.2−0.5. The final concentration of UAA in each culture was 1 mM. Negative control cultures, containing no UAA, of the mutant proteins were grown simultaneously. When cultures reached an optical density between 5.5 and 7.5, protein expression was induced by addition of L-arabinose to a final concentration of 0.2%. Cultures were then incubated at 37 °C for an additional 4 h prior to centrifugation.

Cell pellets were resuspended in wash buffer (100 mM NaCl, 20 mM phosphate, pH 7). The cells were lysed using sonication, and cellular debris was removed by centrifugation. Washed Cobalt Talon resin was added to the clarified samples (5 mL bed volume/L of culture of wtT4 growth, 4.5 mL bed volume/L of culture of T4-153-pENPhe growth, 1.5 mL bed volume/L of culture of T4-153-pCNPhe growth, and 1.5 mL bed volume/L of culture of T4-153 without UAA). Affinity binding took place at room temperature for 1 h with gentle rocking. The resin for each sample was washed with wash buffer until no measurable protein was present in the flow-through, as determined by Coomassie Bradford assay (absorbance ≤0.02). Protein was eluted from the column using elution buffer (100 mM NaCl, 20 mM phosphate, 150 mM imidazole, pH 7). All samples were prepared for fluorescent studies by desalting into assay buffer (20 mM sodium phosphate, 100 mM NaCl, pH 7.0) using PD10 gel filtration columns. Protein concentrations were determined using the Coomassie protein assay kit (Pierce 1856209). Incorporation of the UAAs and protein purity were assessed on 10−20% Tris−glycine SDS−PAGE gels.

Mass Spectrometry Protein Sample Preparation. All protein samples processed for MS analysis were the same protein samples used for fluorescent studies. The samples in assay buffer were exchanged into 20 mM ammonium acetate buffer, pH 7, using PD10 gel filtration columns. Proteins in 20 mM ammonium acetate buffer were lyophilized overnight on a vacuum line. Protein samples for full protein mass spectrometry were resuspended in 1:1 water:acetonitrile with 0.2% formic acid. The samples were analyzed at the Mass Spectrometry Facility at the University of Illinois Urbana−Champaign under the direction of Dr. Furong Sun using their ESI-Q-Tof Ultima (Supporting Information Figure S1). Protein samples for MS/MS fragmentation of tryptic digests were resuspended in 50 mM Tris-HCl buffer, pH 7.0. Sequencing grade trypsin in 100 mM Tris-HCl buffer, pH 7.0, was added to each protein sample, and the samples were incubated at 37 °C overnight. MS analyses were performed on an Agilent 1100 series LC/MSD SL ion trap mass spectrometer with electrospray ionization and MS/MS capabilities. Protein digests (10 μL) were injected onto a Zorbax 300SB-C8 column (narrow bore, 2.1 × 150 mm, 5 μm) for separation using a gradient of 5−85% acetonitrile (with 0.1% formic acid) in water (with 0.1% formic acid) over 75 min. The flow rate was set to 0.25 mL/min. The SL Trap MS was operated in the SPS mode under the normal scan setting. The dry temperature was 325 °C, with a dry gas flow of 10.0 L/min and a nebulizer pressure of 40 psi. For the MS/MS experiments, the instrument was operated in the auto MS/MS mode, selecting two precursor ions with preference given to doubly charged ions while singly charged ions were excluded.

Sample Preparation. The absorbance and emission spectra of the amino acids were recorded in assay buffer. The emission measurements of T4-153-pCNPhe, T4-153-pENPhe, and wtT4 were recorded in assay buffer titrated with urea (MP Biomedicals). The concentrations of the urea solutions were determined by the refractive index of the solutions as previously described (*50*). The solutions for the fluorescence measurements had a protein concentration of 10 μM.

Equilibrium UV/Vis Absorbance Measurements. Equilibrium UV/vis absorbance spectra were recorded on a PerkinElmer Lambda 25 UV/vis spectrometer using a 1 cm quartz sample holder. The spectra were recorded at 23 °C with 1 nm increments and a scan speed of 240 nm/min.

Equilibrium Fluorescence Measurements. Equilibrium fluorescence measurements were recorded on a HORIBA Jobin Yvon Fluoro-Max-4 spectrometer with an excitation bandwidth of 2 nm and an emission bandwidth of either 2 or 5 nm at 23 °C. The spectra were recorded with an integration time of either 1 or 2 s/nm in a 1 cm quartz sample holder. The urea-induced denaturations of T4-153-pCNPhe and T4-153-pENPhe were recorded with an excitation wavelength of 240 nm and an emission wavelength of 297 nm. The urea-induced denaturation of wtT4 was recorded with an excitation wavelength of either 240 or 280 nm and an emission wavelength of either 297 or 360 nm, respectively.

Forster Distance Calculation. The Forster distance, R_0, for the pENPhe/Trp FRET pair, in units of angstroms, was determined based upon eq 1 (*51*):

$$R_0 = 0.211(\kappa^2 \eta^{-4} Q_D J(\lambda))^{1/6} \quad (1)$$

where κ^2 is an orientation factor and taken to be $^2/_3$ in this study, η is the refractive index of the medium which is 1.33 in this study, and Q_D is the fluorescence quantum yield of the donor, pENPhe. The overlap integral, $J(\lambda)$, is given by eq 2 (*51*):

$$J(\lambda) = \frac{\int_0^\infty F_D(\lambda)\varepsilon_A(\lambda)\lambda^4 \, d\lambda}{\int_0^\infty F_D(\lambda) \, d\lambda} \quad (2)$$

where λ is the wavelength, $F_D(\lambda)$ is the emission spectrum of the donor (pENPhe), and $\varepsilon_A(\lambda)$ is the wavelength-dependent molar absorption coefficient of the acceptor (Trp). The quantum yield of the donor, Q_D, was determined using eq 3 (*51*):

$$Q_D = Q_R \frac{I_D}{I_R} \left(\frac{A_R(\lambda_{ex})}{A_D(\lambda_{ex})} \right) \frac{{\eta_D}^2}{{\eta_R}^2} \quad (3)$$

where Q_R is the quantum yield of the reference, I_D and I_R are the integrated fluorescence intensities of the donor and reference, respectively, $A_D(\lambda_{ex})$ and $A_R(\lambda_{ex})$ are the absorbance at the excitation wavelength of the donor and reference, respectively, and ${\eta_D}^2$ and ${\eta_R}^2$ are the refractive index of the medium for the donor and reference, respectively.

Protein Stability Calculation. The protein denaturation curves showing the dependence of the measured emission intensity, $I_{measured}$, on urea concentration, C, were fit to a two-state model given by eq 4:

$$I_{measured} = \frac{(a_f + b_f C) - (a_u + b_u C)}{1 + e^{-m(C_m - C)/RT}} + (a_u + b_u C) \quad (4)$$

where $(a_f + b_f C)$ and $(a_u + b_u C)$ represent the linear urea dependence of the fluorescence of the folded and unfolded states, respectively, where a_f and a_u are intercepts and b_f and b_u are slopes, C_m is the denaturant concentration at the midpoint of the unfolding transition, R is the gas constant, and T is the temperature. The m parameter relates the linear dependence of the standard change in the Gibbs energy for the unfolding process on denaturant concentration as shown in eq 5:

$$\Delta G^\circ_u = \Delta G^\circ_u(H_2O) - mC \quad (5)$$

where ΔG°_u and $\Delta G^\circ_u(H_2O)$ are the standard change in the Gibbs energy for the unfolding process in the presence or absence of denaturant, respectively. This linear dependence of ΔG°_u is inherent in the derivation of eq 4. The standard change in Gibbs free energy for the unfolding process (i.e., the stability of the protein) in the absence of denaturant (urea), $\Delta G^\circ_u(H_2O)$ can be determined based on eq 6:

$$\Delta G^\circ_u(H_2O) = mC_m \quad (6)$$

where m and C_m are determined from the fit of eq 4 to the experimentally measured denaturation curves of the protein constructs. The data analysis was performed with IGOR Pro (Wavemetrics, Inc.).

RESULTS AND DISCUSSION

Photophysics of pCNPhe and pENPhe. Figure 2 illustrates the potential of the unnatural amino acids, pCNPhe and pENPhe, to participate in fluorescence resonance energy transfer (FRET) as donors with the natural amino acid Trp as the acceptor. Figure 2A shows the concentration-normalized absorbance spectra of pCNPhe, pENPhe, and Trp in buffer (20 mM sodium phosphate, 100 mM sodium chloride, pH 7.0) in the 210−310 nm region. In this region, the absorbance spectrum of pCNPhe contains a prominent maximum at 230 nm, while pENPhe has two prominent maxima at 240 and 250 nm. Trp exhibits two prominent absorbance bands centered at 218 and 279 nm, with a minimum between these bands at 243 nm. Consequently, both UAAs can be preferentially excited around 243 nm, where they exhibit similar molar absorptivities, in the presence of Trp. Additionally, pENPhe can also be

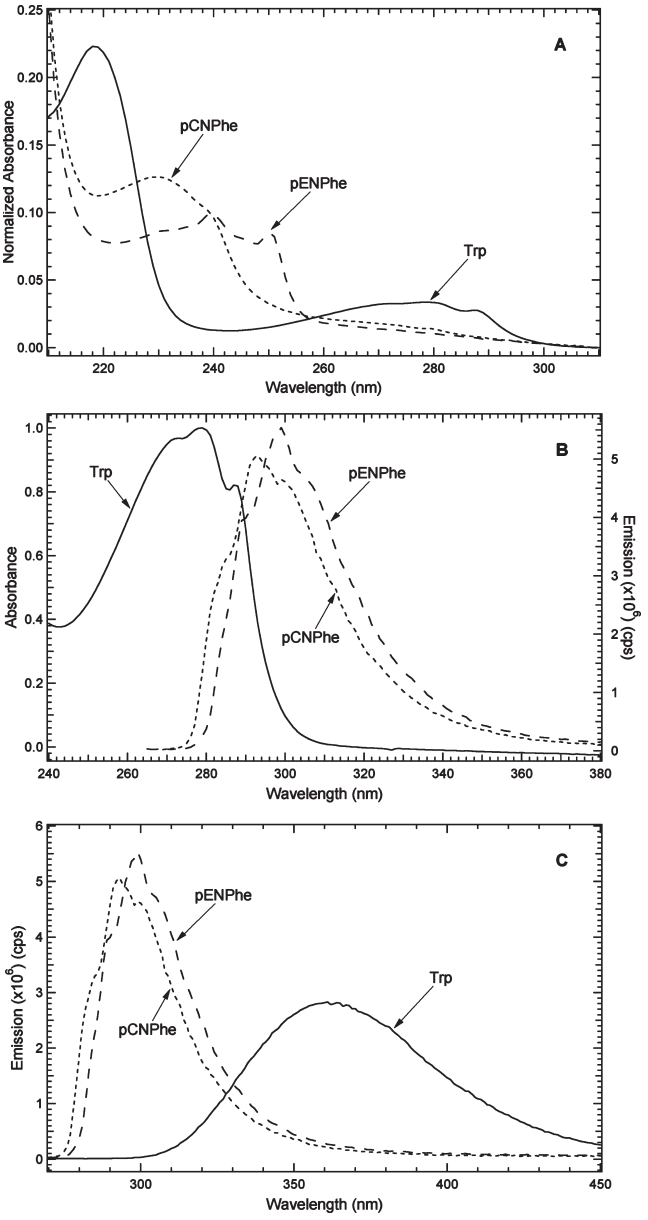

FIGURE 2: (A) Absorbance spectra of the unnatural amino acids, pCNPhe (short-dashed curve) and pENPhe (long-dashed curve), and the natural amino acid, Trp (solid curve), normalized by concentration. (B) Absorbance spectrum of Trp (solid curve) overlaid with the emission spectra of pCNPhe (short-dashed curve) and pENPhe (long-dashed curve). (C) Emission spectra of the three amino acids: pCNPhe (short-dashed curve), pENPhe (long-dashed curve), and Trp (solid curve). The emission spectra were the result of excitation at 240 nm.

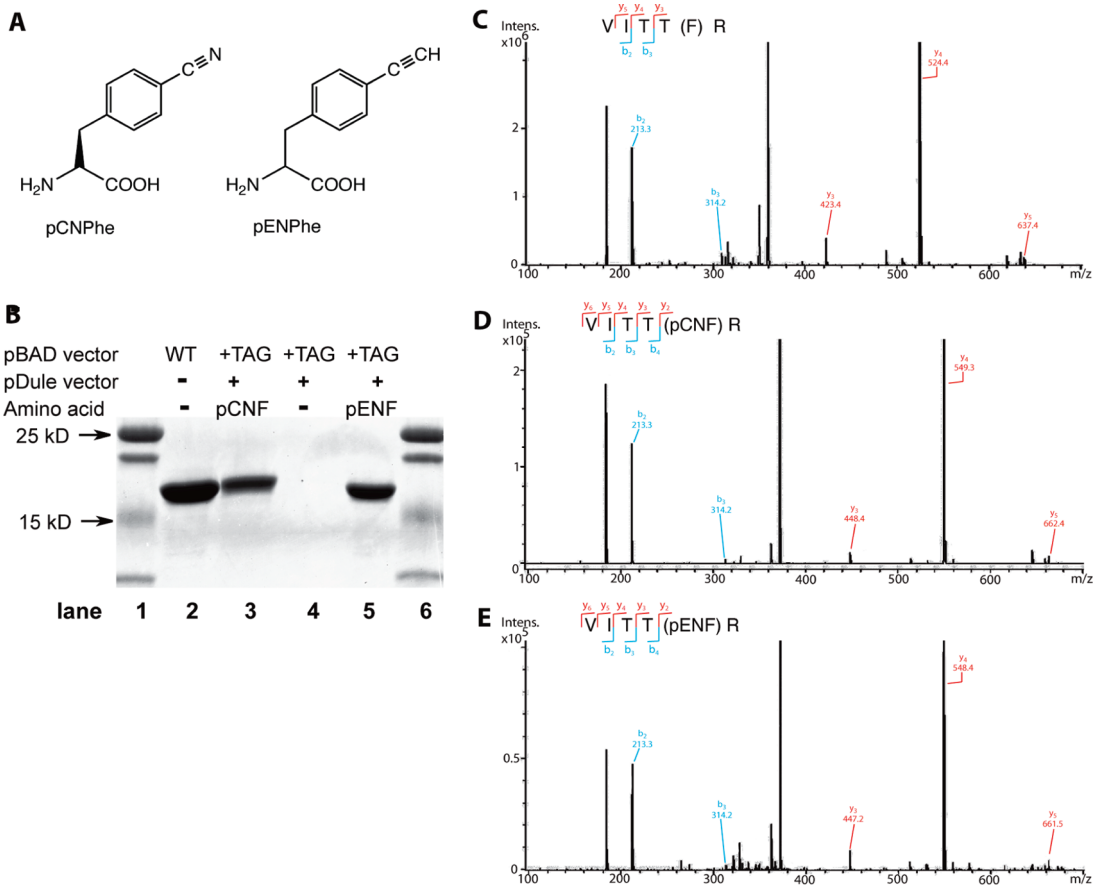

FIGURE 3: SDS−PAGE and MS analysis of T4 lysozyme demonstrate the efficient and site-specific incorporation of pCNPhe and pENPhe in response to the amber stop codon. (A) Structures of L-4-cyanophenylalanine (pCNPhe) and 4-ethynylphenylalanine (pENPhe). (B) T4 lysozyme was expressed from plasmids *pBad-T4* (wtT4, lane 2), or *pBad-T4-153TAG* and *pDule-pspPhe* (lanes 3−5). The same cells were used to express protein in the presence of 1 mM pCNPhe (lane 3), in the absence of UAA (lane 4), and in the presence of 1 mM pENPhe (lane 5). Proteins were purified in parallel by affinity chromatography, analyzed by SDS−PAGE, and stained with Coomassie blue. (C) MS/MS fragmentation of the only tryptic peptide with MS^{+2} (369.2) derived from wtT4. (D) MS/MS fragmentation of the only tryptic peptide with MS^{+2} (381.4) derived from T4-153-pCNPhe. (E) MS/MS fragmentation of the only tryptic peptide with MS^{+2} (381.1) derived from T4-153-pENPhe. (C−E) The spectra confirm the incorporation of pCNPhe and pEFPhe at residue 153. The fragmentation sites are illustrated above the spectra.

selectively excited at 250 nm due to its relatively high molar absorptivity at this wavelength relative to Trp, unlike pCNPhe, offering a potential advantage of using pENPhe over pCNPhe.

Figure 2B shows the comparison of the emission spectra of pCNPhe and pENPhe resulting from excitation at 240 nm with the absorbance spectrum of Trp. The excitation wavelength was chosen so that both UAAs could be directly compared, due to their high molar extinction coefficients at this wavelength relative to Trp, as well as for consistency with previous studies of pCNPhe.(*13*) The emission spectra of pCNPhe and pENPhe show emission maxima at 293 and 299 nm, respectively, with similar emission intensities. The quantum yield of pENPhe was determined to be 0.09 ± 0.01 using eq 3 with tyrosine (quantum yield = 0.14)(*51*) and pCNPhe (quantum yield = 0.11) (*13*) as references.

The emission spectra of both UAAs show significant overlap between their emission spectra and the absorbance spectra of Trp. This overlap is required to achieve efficient resonance energy transfer between pCNPhe or pENPhe with Trp, given the residues are sufficiently close in distance. The Forster distance, R_0, for the pENPhe/Trp FRET pair was determined using eqs 1 and 2 to be 15.6 ± 0.3 Å, which is similar to the previously reported Forster distance of the pCNPhe/Trp FRET pair, 16.0 ± 0.5 Å (*13*).

Figure 2C shows the emission spectra of pCNPhe, pENPhe, and Trp with an excitation wavelength at 240 nm. The emission maximum of Trp is 361 nm, which is significantly red shifted from the emission maximum of pCNPhe and pENPhe. Consequently, the emission of the UAAs can be selectively measured at 297 nm with minimal interference from the emission of Trp. This characteristic allows the efficiency of FRET between pCNPhe or pENPhe with Trp to be measured since the observed fluorescence of the donor will increase as the FRET efficiency decreases.

The small size of the ethynyl and cyano groups of pENPhe and pCNPhe, respectively (Figure 3A), suggests that replacing a phenylalanine residue for either of these two UAAs in a protein should be well tolerated by the native structure of the protein. The two UAAs, however, do exhibit some chemical differences. The small size of the cyano moiety and its intermediate polarity likely explain the minimal perturbation in peptide structure that results from pCNPhe incorporation (*13*, *14*). The pENPhe residue is less polar than the pCNPhe residue, suggesting that substitution of this residue into the hydrophobic core of proteins might be better tolerated than pCNPhe. Another notable difference between the residues is the ability of the cyano group of pCNPhe to form hydrogen-bonding interactions with solvent, unlike pENPhe. This distinction suggests that pCNPhe might be more sensitive to small changes in polar environments, while pENPhe might be more sensitive to small changes in nonpolar

environments, such as in the hydrophobic core of proteins. These sensitivities to electrostatic environment are also suggested by emission measurements of the two unnatural amino acids in solvents of varying polarity (data not shown).

Selection of para-sp-Phenylalanine Specific Aminoacyl-tRNA Synthetase. An aminoacyl-tRNA synthetase that could site-specifically incorporate a phenylalanine amino acid containing a general sp hybridized functionality in the para position would be of great utility for protein IR studies, fluorescence studies, and chemical ligations. This report focuses on the ability to incorporate 4-ethynylphenylalanine (pENPhe). To evolve an aminoacyl-tRNA synthetase for the site-specific incorporation of para-sp hybridized phenylalanine functionalized amino acids, we began with a modified *M. jannaschii* (*Mj*) tyrosyl-tRNA synthetase/$tRNA_{CUA}$ pair, which directs the incorporation of tyrosine in response to the amber (UAG) codon (*36*, *47*). This pair is orthogonal to the endogenous aminoacyl-tRNA synthetases and tRNAs in *E. coli*: *Mj* tyrosyl-tRNA synthetase does not appreciably aminoacylate endogenous tRNAs, and *Mj* $tRNA_{CUA}$ is not aminoacylated by endogenous aminoacyl-tRNA synthetases. We used a library of the gene for this synthetase in which codons corresponding to six amino acid residues (Tyr32, Leu65, Phe108, Gln109, Asp158, Ile159) within 7 Å of the bound tyrosine in the active site were randomized (*47*). Since the desired amino acid for incorporation, pENPhe, is not commercially available and could have mild toxicity, we chose to obtain an aminoacyl-tRNA synthetase capable of incorporating pENPhe by performing selections in the presence of the molecular surrogate L-4-cyanophenylalanine (pCNPhe). Schultz et al. have previously selected a synthetase capable of incorporating pCNPhe generating the plasmid *pSup-CNPheRS-6TRN* (*37*). Attempts to produce T4-153-pENPhe with *pSup-CNPheRS-6TRN* and *pBad-T4-153TAG* resulted in no incorporation of pENPhe into T4 lysozyme. Previous experiments in our laboratory suggest that molecular surrogate incorporation is more successful if all top synthetase clones from a selection are assessed for incorporation (*32*). On this premise, the synthetase library was subjected to three rounds of alternating positive and negative selections in the presence and absence of pCNPhe, respectively.

Of the resulting aminoacyl-tRNA synthetase clones, 40 were isolated and transformed into cells bearing *pREP2-JYCUA*, which contains *Mj* $tRNA_{CUA}$ and confers amber suppressor dependent expression of green fluorescent protein and chloramphenicol acetyl transferase on *E. coli*. All synthetase clones showed amino acid dependent expression of both reporters, surviving at Cm concentrations of 120 μg/mL in the presence of pCNPhe but only at concentrations of less than 15 μg/mL in the absence of pCNPhe. Sequencing ten distinct clones revealed that all contained the identical sequence (Leu32, Val65, Trp108, Met109, Gly158, Pro159).

For further characterization of the incorporation of pCNPhe and pENPhe into proteins in response to the amber codon, we cloned the single synthetase clone into a *pDule* vector that contains one copy of *Mj* $tRNA_{CUA}$ to create *pDule-pspPhe*. We cotransformed *pDule-pspPhe* with *pBad-T4-153TAG*, which contains the gene encoding T4 lysozyme with an amber codon at position 153 and a C-terminal 6-His affinity tag. We expressed protein from *pBad-T4-153TAG* in the presence and absence of pCNPhe and pENPhe and purified 6-His-tagged protein via cobalt affinity chromatography. In the presence of 1 mM L-pCNPhe, full-length T4 lysozyme could be purified with a yield of 7.5 mg/L, while no T4 lysozyme was purified in the absence of amino acid (Figure 3B). To assess the ability of synthetase that incorporates pCNPhe to incorporate similar structural analogues, parallel identical expression was performed in the presence of 1 mM racemic pENPhe. The yield of T4 containing pENPhe at site 153 (T4-153-pENPhe) was 23 mg/L of pure protein, consistently three times that of the T4-153-pCNPhe protein yield. Wild-type T4 lysozyme protein (wtT4) yields were consistently 30 mg/L under identical expression conditions (Figure 3B).

For further confirmation of the incorporation of pCNPhe and pENPhe, the mass of wtT4 was compared with that of T4-153-pCNPhe and T4-153-pENPhe using ESI-Q-Tof mass analysis. The difference in mass observed between wtT4 and T4-153-pCNPhe (25 ±1 Da) corresponds to a single nitrile group, and the difference between wtT4 and T4-153-pENPhe (24 ±1 Da) corresponds to a single ethynyl group (Supporting Information Figure S1). For further verification that the single pCNPhe and pENPhe were incorporated in place of Phe153, the proteins wtT4, T4-153-pCNPhe, and T4-153-pENPhe were subjected to trypsin digest followed by LC and tandem mass spectrometry (MS/MS) analysis (Figure 3C−E). Overall, the results of protein expression with affinity purification and SDS−PAGE, MS, and MS/MS analysis demonstrate the high fidelity and site-specific incorporation of pCNPhe and pENPhe at genetically programmed sites in T4 lysosyme using *pDule-pspPhe*.

FRET Monitored Denaturation of T4 Lysozyme. His-tagged T4 lysozyme is a 171-residue monomeric protein composed of 65% helical structure and 9% β-sheet structure as shown in Figure 1. Here, we have substituted Phe153 in the core of the protein with either pCNPhe or pENPhe. Previous studies on the $\alpha-\beta$ 56-residue NTL9 peptide showed that the substitution of Phe with pCNPhe in the hydrophobic core was well tolerated (*14*). This would suggest that the substitution of Phe153 with pCNPhe should be well tolerated in T4 lysozyme. The less polar nature and similar size of pENPhe compared to pCNPhe would also suggest that the 153-pENPhe substitution should also be well tolerated. The Phe153 residue is in relatively close proximity to the three Trp residues in the native state of the protein. The $C\beta-C\beta$ distances between Phe153 and Trp126, Trp138, and Trp158 are 6Å, 13, and 12 Å, respectively. If we assume an extended conformation for the unfolded state and 3.8 Å between the Cα atoms of neighboring residues, then the $C\alpha-C\alpha$ distance between Phe153 and Trp126, Trp138, and Trp158 are 103, 57, and 19 Å, respectively. Therefore, the $C\beta-C\beta$ distances between Phe153 and the three Trp residues are within the Forster distance in the native state for both the pCNPhe/Trp and pENPhe/Trp FRET pair, with the change in distance between Phe153 and Trp126 being the largest upon unfolding the protein. Consequently, resonance energy transfer of varying efficiencies is likely to occur between Phe153 and each of the Trp residues in the folded state of the protein, while no resonance energy transfer is expected between Phe153 and Trp126 (and potentially Trp138) in the unfolded state of the protein. However, there is likely some FRET between Phe153 and Trp158 in the unfolded state. Consequently, the observed emission of the donor UAAs should increase upon unfolding of the protein as the distances between the donors (pENPhe or pCNPhe) and the acceptors (Trp126, Trp138, and Trp158) increase, thereby decreasing the efficiency of resonance energy transfer between the donor and acceptor molecules. The observed change in the emission of the donor UAAs will likely be partially suppressed by the potential for FRET between Phe153 and Trp158 in both the folded and unfolded states of the protein.

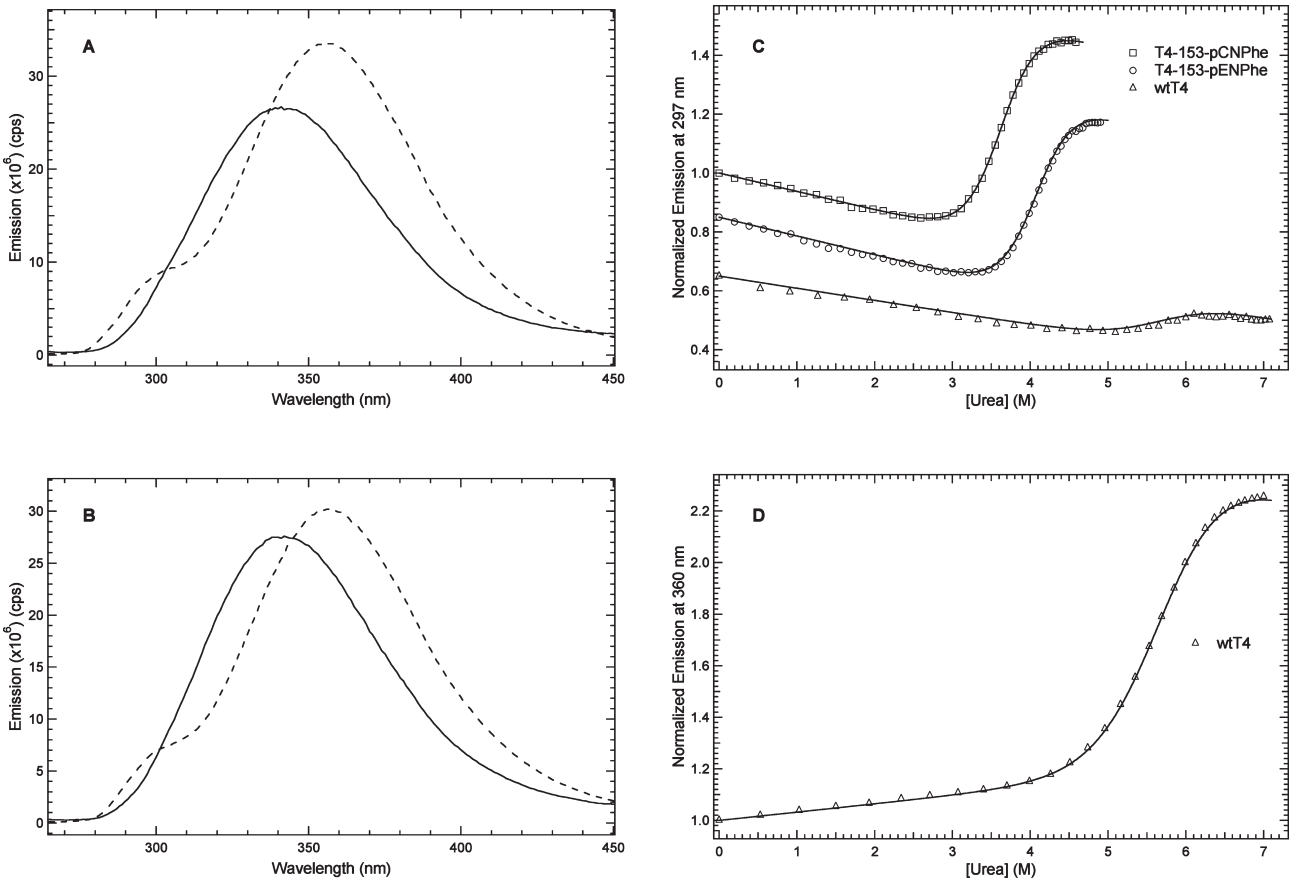

FIGURE 4: (A, B) Emission spectra corresponding to the folded (solid curves) and urea-induced unfolded (dashed curves) states for T4-153-pCNPhe (A) and T4-153-pENPhe (B) with an excitation of 240 nm. (C) Emission intensity measured at 297 nm due to excitation at 240 nm as a function of urea concentration for T4-153-pCNPhe (open squares), T4-153-pENPhe (open circles), and wtT4 (open triangles) with the corresponding fits (solid curves) from a two-state model. (D) Emission intensity measured at 360 nm due to excitation at 280 nm as a function of urea concentration for wtT4 (open triangles) with the corresponding fit (solid curve) to a two-state model. The emission intensities were normalized to the initial emission in the absence of urea and offset (C) for comparison.

Panels A−C of Figure 4 show the change in FRET efficiency between pCNPhe/Trp and pENPhe/Trp upon the urea-induced denaturation of T4-153-UAA. Panels A and B of Figure 4 show the emission spectra corresponding to the folded (solid curve) and urea-induced unfolded (dashed curves) states for T4-153-pCNPhe and T4-153-pENPhe with an excitation of 240 nm, respectively. These spectra show an increase in the fluorescence at 297 nm due to a decrease in the FRET efficiency between pCNPhe/Trp (A) and pENPhe/Trp (B) upon urea-induced denaturation of T4-153-UAA. The spectra also show an increase in tryptophan emission and a red shift in the tryptophan emission maximum from 342 to 357 nm upon unfolding.

Figure 4C highlights the change in FRET efficiency between pCNPhe/Trp (open squares) and pENPhe/Trp (open circles) upon the urea-induced denaturation of T4-153-UAA. These two denaturation curves show an increase in the emission at 297 nm with increasing urea concentration, resulting primarily from the selective excitation of either pCNPhe or pENPhe at 240 nm. The increase in fluorescence in the transition region of the curves in Figure 4C is due to a decrease in the efficiency of fluorescence resonance energy transfer between pCNPhe153 and Trp (open squares) and pENPhe153 and Trp (open circles) resulting in a larger observed emission of the UAAs at 297 nm. The background emission from tyrosine and tryptophan residues in the protein at 297 nm is shown in the denaturation curve for wtT4 (open triangles) in Figure 4C with an excitation wavelength of 240 nm. This curve shows there is minimal observed emission at 297 nm from tyrosine and tryptophan residues in the denaturation curves for T4-153-pCNPhe and T4-153-pENPhe. The observed transition for wtT4 is likely due to the intrinsic quantum yield dependence of primarily tyrosine residues as the protein unfolds. All three denaturation curves show the same negative sloping pretransition baseline, which is probably due primarily to the urea dependence of the quantum yield of tyrosine. The three denaturation curves were normalized to the initial emission intensity in the absence of urea and stacked for ease of comparison.

Figure 4C demonstrates the utility of these two FRET pairs in protein systems to yield information about the average distance between the donor and acceptors at micromolar protein concentrations with a nondestructive spectroscopic technique. Both UAAs show a similar dynamic range, suggesting a similar sensitivity to the change in the average distance between Phe153 and the three Trp residues in the protein. For a more quantitative description of the results, the denaturation curves in Figure 4C were fit to eq 4 (solid curves) assuming a two-state model of unfolding. The resulting fit parameters are given in Table 1. The m value is correlated with change in the solvent-accessible surface area between the folded and unfolded state of the protein. The m values for both of the unnatural T4 protein constructs are similar, which suggests that pCNPhe and pENPhe are in the same local environment, as expected since residue 153 is in the hydrophobic core of the protein. The C_m value is the midpoint of the urea-induced denaturation of the protein constructs. The C_m value for

Table 1: Values from the Fit of the Urea-Induced Denaturation Curves for T4-153-pCNPhe, T4-153-pENPhe, and wtT4 Using Equation 4[a]

	m (kcal L/mol^2)	C_m (M)	$\Delta G°_u(H_2O)$ (kcal/mol)
T4-153-pCNPhe	2430 ± 70	3.63 ± 0.02	8.8 ± 0.3
T4-153-pENPhe	2400 ± 100	4.10 ± 0.02	10.0 ± 0.6
wtT4	1430 ± 70	5.68 ± 0.06	8.2 ± 0.5

[a] The reported standard deviations are the result of measuring the denaturation curves in triplicate.

T4-153-pCNPhe is 0.47 M less than T4-153-pENPhe. Consequently, the standard change in the Gibbs energy for the unfolding process in the absence of denaturant $\Delta G°_u(H_2O)$ is 8.8 ± 0.3 kcal/mol for T4-153-pCNPhe compared to 10.0 ± 0.6 kcal/mol for T4-153-pENPhe, suggesting that T4-153-pENPhe is more stable than T4-153-pCNPhe.

Figure 4D shows the denaturation curve for wtT4 measured by directly exciting the Trp residues at 280 nm and monitoring the Trp emission at 360 nm. The increase in fluorescence is due to the change in the quantum yield of Trp as protein unfolding changes the local environments of the residues. The results for the fit of the experimental data to eq 4 are given in Table 1. These values are consistent with the results to the fit of the denaturation curve of wtT4 in Figure 4A. The fit yields a smaller m value compared to the two UAA constructs, suggesting a smaller change in the solvent-accessible surface area of the Trp residues upon unfolding. This result is consistent with the crystal structure of T4 lysozyme (Figure 1), which shows that both Trp126 and Trp158 are at least partially solvated in the folded state. The m and C_m values from the fit yield a change in the standard Gibbs energy for the unfolding process in the absence of denaturant of 8.2 ± 0.5 kcal/mol.

The measured stabilities of T4-153-pCNPhe and T4-153-pENPhe relative to wtT4 show that both the pCNPhe and pENPhe substitutions in the hydrophobic core of the protein are well tolerated. The standard change in the Gibbs energy for unfolding in the absence of denaturant for the pCNPhe construct is within the experimental error of $\Delta G°_u(H_2O)$ for wtT4. The $\Delta G°_u(H_2O)$ value for the pENPhe construct is slightly higher than $\Delta G°_u(H_2O)$ for wtT4. These results suggest that the pCNPhe substitution did not alter the stability of the protein, while the pENPhe substitution resulted in a slightly more stable protein. This slight increase in measured stability could result from the hydrophobic nature of the ethynyl group of pENPhe or from using a two-state model to fit the denaturation of the protein. While this model does fit the measured data, the protein might unfold through a more complicated mechanism, impacting the measured stability of the protein constructs. Regardless of the effects on stability, the data clearly show that either pCNPhe or pENPhe can be used as FRET donors with Trp as the acceptor to measure conformational changes in proteins as demonstrated here by monitoring the urea-induced unfolding of T4 lysozyme.

CONCLUSIONS

Site-specifically encoded UAAs were shown to be effective FRET donors with Trp to study protein folding. An aminoacyl-tRNA synthetase/tRNA pair for the cotranslational, site-specific incorporation of the UAAs into proteins at genetically encoded sites was selected. This single set of genetic machinery permitted the incorporation of either pCNPhe or pENPhe into proteins. The photophysics of the UAAs showed that the residues could participate as donors in fluorescence resonance energy transfer with Trp as the acceptor, due to the overlap between the emission spectra of the UAAs with the absorbance band of Trp. Additionally, the UAAs could be selectively excited and their emission could be selectively monitored, which are additional requirements for FRET donors. The UAAs were incorporated into the hydrophobic core of wtT4 at site 153 in close proximity to three Trp residues in the native state. Upon urea-induced unfolding, the average distance between the donor and acceptors increased, thus decreasing the FRET efficiency. An increase in the observed emission of the UAAs was observed upon the unfolding of the protein, confirming that both pCNPhe and pENPhe can act as FRET donors with Trp in a protein system. The pENPhe and Trp FRET pair had not been previously reported. Previous studies with the pCNPhe and Trp FRET pair were performed solely with peptides made by standard solid-phase peptide synthetic protocols. This study represents the first example of either FRET pair being used to probe protein unfolding in proteins.

The replacement of Phe153 for either pCNPhe or pENPhe was well tolerated by T4 lysozyme. The conservative nature of the pCNPhe substitution in the hydrophobic core of T4 lysozyme is likely due to the small size and the intermediate polarity of the cyano group. The pENPhe substitution into the hydrophobic core resulted in a slightly more stable T4 protein, which is likely related to the comparable size and greater hydrophobicity of the ethynyl group. These results suggest that the incorporation of pENPhe into the hydrophobic core of proteins will be more favorable than the incorporation of pCNPhe.

This methodology of using site-specifically encoded UAAs as FRET donors to probe conformational changes in proteins is generally applicable. There is no inherent protein size limitation for the incorporation of the unnatural amino acids. The two amino acids, pCNPhe and pENPhe, represent conservative replacements for phenylalanine residues and, potentially, for other aromatic residues. FRET has the ability to measure distances between the donor and acceptor molecules, which can be utilized to probe conformational changes involved in protein folding, protein aggregation, protein−protein interactions, ligand binding to proteins, and protein−DNA interactions. FRET utilizes fluorescence spectroscopy that is advantageous due to its high sensitivity, permitting protein studies in the micromolar concentration regime, with a temporal resolution that is sufficient to study protein dynamics on all relevant time scales. The combination of the site-specific incorporation methodology for the unnatural amino acids into proteins, along with the ability of the UAAs acids to participate in FRET as donors with Trp residues, results in a general method for the study of protein conformational changes. The intermediate polarity of the cyano group makes pCNPhe a suitable FRET donor for incorporation into either the hydrophobic core or a solvated site in proteins, while the hydrophobic nature of the ethynyl group suggests that pENPhe is the preferred FRET donor for incorporation into the hydrophobic core of proteins, so that protein conformational changes can be probed in the least intrusive manner.

ACKNOWLEDGMENT

We thank Beth Buckwalter and Carol Strausser for technical assistance. We gratefully acknowledge the help of Lisa Mertzman, Nathan George, and Miles Gibson.

SUPPORTING INFORMATION AVAILABLE

A description of the mass spectrometry of proteins, synthesis of 4-ethynylphenylalanine, and emission spectra of the folded and unfolded states of the protein constructs. This material is available free of charge via the Internet at http://pubs.acs.org.

REFERENCES

1. Chiti, F., and Dobson, C. M. (2006) Protein misfolding, functional amyloid, and human disease. *Annu. Rev. Biochem. 75*, 333–366.
2. Fersht, A. R. (2000) Structure and Mechanism in Protein Science: A Guide to Enzyme Catalysis and Protein Folding , W. H. Freeman, New York.
3. Onuchic, J. N., Nymeyer, H., Garcia, A. E., Chahine, J., and Socci, N. D. (2000) The energy landscape theory of protein folding: Insights into folding mechanisms and scenarios. *Adv. Protein Chem. 53*, 87–152.
4. Selkoe, D. J. (2003) Folding proteins in fatal ways. *Nature 426*, 900–904.
5. Snow, C. D., Qiu, L. L., Du, D. G., Gai, F., Hagen, S. J., and Pande, V. S. (2004) Trp zipper folding kinetics by molecular dynamics and temperature-jump spectroscopy. *Proc. Natl. Acad. Sci. U.S.A. 101*, 4077–4082.
6. Duan, Y., and Kollman, P. A. (1998) Pathways to a protein folding intermediate observed in a 1-microsecond simulation in aqueous solution. *Science 282*, 740–744.
7. Brewer, S. H., Vu, D. M., Tang, Y. F., Li, Y., Franzen, S., Raleigh, D. P., and Dyer, R. B. (2005) Effect of modulating unfolded state structure on the folding kinetics of the villin headpiece subdomain. *Proc. Natl. Acad. Sci. U.S.A. 102*, 16662–16667.
8. Getahun, Z., Huang, C. Y., Wang, T., De Leon, B., DeGrado, W. F., and Gai, F. (2003) Using nitrile-derivatized amino acids as infrared probes of local environment. *J. Am. Chem. Soc. 125*, 405–411.
9. Mikhonin, A. V., and Asher, S. A. (2006) Direct UV Raman monitoring of 3(10)-helix and pi-bulge premelting during alpha-helix unfolding. *J. Am. Chem. Soc. 128*, 13789–13795.
10. Wang, M. H., Tang, Y. F., Sato, S. S., Vugmeyster, L., McKnight, C. J., and Raleigh, D. P. (2003) Dynamic NMR line-shape analysis demonstrates that the villin headpiece subdomain folds on the microsecond time scale. *J. Am. Chem. Soc. 125*, 6032–6033.
11. Godoy-Ruiz, R., Henry, E. R., Kubelka, J., Hofrichter, J., Munoz, V., Sanchez-Ruiz, J. M., and Eaton, W. A. (2008) Estimating free-energy barrier heights for an ultrafast folding protein from calorimetric and kinetic data. *J. Phys. Chem. B 112*, 5938–5949.
12. Kubelka, J., Eaton, W. A., and Hofrichter, J. (2003) Experimental tests of villin subdomain folding simulations. *J. Mol. Biol. 329*, 625–630.
13. Tucker, M. J., Oyola, R., and Gai, F. (2005) Conformational distribution of a 14-residue peptide in solution: A fluorescence resonance energy transfer study. *J. Phys. Chem. B 109*, 4788–4795.
14. Aprilakis, K. N., Taskent, H., and Raleigh, D. P. (2007) Use of the novel fluorescent amino acid rho-cyanophenylalanine offers a direct probe of hydrophobic core formation during the folding of the N-terminal domain of the ribosomal protein L9 and provides evidence for two-state folding. *Biochemistry 46*, 12308–12313.
15. Fang, C., Wang, J., Kim, Y. S., Charnley, A. K., Barber-Armstrong, W., Smith, A. B.III, Decatur, S. M., and Hochstrasser, R. M. (2004) Two-dimensional infrared spectroscopy of isotopomers of an alanine rich alpha-helix. *J. Phys. Chem. B 108*, 10415–10427.
16. Huang, C. Y., Getahun, Z., Zhu, Y. J., Klemke, J. W., DeGrado, W. F., and Gai, F. (2002) Helix formation via conformation diffusion search. *Proc. Natl. Acad. Sci. U.S.A. 99*, 2788–2793.
17. Huang, R., Kubelka, J., Barber-Armstrong, W., Silva, R. A. G. D., Decatur, S. M., and Keiderling, T. A. (2004) Nature of vibrational coupling in helical peptides: An isotopic labeling study. *J. Am. Chem. Soc. 126*, 2346–2354.
18. Werner, J. H., Dyer, R. B., Fesinmeyer, R. M., and Andersen, N. H. (2002) Dynamics of the primary processes of protein folding: Helix nucleation. *J. Phys. Chem. B 106*, 487–494.
19. Brewer, S. H., Song, B. B., Raleigh, D. P., and Dyer, R. B. (2007) Residue specific resolution of protein folding dynamics using isotope-edited infrared temperature jump spectroscopy. *Biochemistry 46*, 3279–3285.
20. Fang, C., Wang, J., Charnley, A. K., Barber-Armstrong, W., Smith, A. B., Decatur, S. M., and Hochstrasser, R. M. (2003) Two-dimensional infrared measurements of the coupling between amide modes of an alpha-helix. *Chem. Phys. Lett. 382*, 586–592.
21. Mukherjee, P., Krummel, A. T., Fulmer, E. C., Kass, I., Arkin, I. T., and Zanni, M. T. (2004) Site-specific vibrational dynamics of the CD3 zeta membrane peptide using heterodyned two-dimensional infrared photon echo spectroscopy. *J. Chem. Phys. 120*, 10215–10224.
22. Torres, J., Briggs, J. A. G., and Arkin, I. T. (2002) Multiple site-specific infrared dichroism of CD3-zeta, a transmembrane helix bundle. *J. Mol. Biol. 316*, 365–374.
23. Religa, T. L., Johnson, C. M., Vu, D. M., Brewer, S. H., Dyer, R. B., and Fersht, A. R. (2007) The helix-turn-helix motif as an ultrafast independently folding domain: The pathway of folding of engrailed homeodomain. *Proc. Natl. Acad. Sci. U.S.A. 104*, 9272–9277.
24. Ma, H. R., and Gruebele, M. (2005) Kinetics are probe-dependent during downhill folding of an engineered lambda(6−85) protein. *Proc. Natl. Acad. Sci. U.S.A. 102*, 2283–2287.
25. Horng, J. C., Tracz, S. M., Lumb, K. J., and Raleigh, D. P. (2005) Slow folding of a three-helix protein via a compact intermediate. *Biochemistry 44*, 627–634.
26. Gustiananda, M., Liggins, J. R., Cummins, P. L., and Gready, J. E. (2004) Conformation of prion protein repeat peptides probed by FRET measurements and molecular dynamics simulations. *Biophys. J. 86*, 2467–2483.
27. Haas, E., Wilchek, M., Katchalskikatzir, E., and Steinberg, I. Z. (1975) Distribution of end-to-end distances of oligopeptides in solution as estimated by energy-transfer. *Proc. Natl. Acad. Sci. U.S.A. 72*, 1807–1811.
28. Schuler, B., Lipman, E. A., and Eaton, W. A. (2002) Probing the free-energy surface for protein folding with single-molecule fluorescence spectroscopy. *Nature 419*, 743–747.
29. Tucker, M. J., Tang, J., and Gai, F. (2006) Probing the kinetics of membrane-mediated helix folding. *J. Phys. Chem. B 110*, 8105–8109.
30. Tang, J., Signarvic, R. S., DeGrado, W. F., and Gai, F. (2007) Role of helix nucleation in the kinetics of binding of mastoparan X to phospholipid bilayers. *Biochemistry 46*, 13856–13863.
31. Glasscock, J. M., Zhu, Y. J., Chowdhury, P., Tang, J., and Gai, F. (2008) Using an amino acid fluorescence resonance energy transfer pair to probe protein unfolding: Application to the villin headpiece subdomain and the LysM domain. *Biochemistry 47*, 11070–11076.
32. Jackson, J. C., Hammill, J. T., and Mehl, R. A. (2007) Site-specific incorporation of a (19)F-amino acid into proteins as an NMR probe for characterizing protein structure and reactivity. *J. Am. Chem. Soc. 129*, 1160–1166.
33. Tsao, M. L., Summerer, D., Ryu, Y., and Schultz, P. G. (2006) The genetic incorporation of a distance probe into proteins in *Escherichia coli*. *J. Am. Chem. Soc. 128*, 4572–4573.
34. Wang, J., Xie, J., and Schultz, P. G. (2006) A genetically encoded fluorescent amino acid. *J. Am. Chem. Soc. 128*, 8738–8739.
35. Wang, L., Brock, A., Herberich, B., and Schultz, P. G. (2001) Expanding the genetic code of *Escherichia coli*. *Science 292*, 498–500.
36. Xie, J., and Schultz, P. G. (2006) A chemical toolkit for proteins—an expanded genetic code. *Nat. Rev. Mol. Cell Biol. 7*, 775–782.
37. Schultz, K. C., Supekova, L., Ryu, Y., Xie, J., Perera, R., and Schultz, P. G. (2006) A genetically encoded infrared probe. *J. Am. Chem. Soc. 128*, 13984–13985.
38. Deiters, A., and Schultz, P. G. (2005) In vivo incorporation of an alkyne into proteins in *Escherichia coli*. *Bioorg. Med. Chem. Lett. 15*, 1521–1524.
39. Strable, E., Prasuhn, D. E.Jr., Udit, A. K., Brown, S., Link, A. J., Ngo, J. T., Lander, G., Quispe, J., Potter, C. S., Carragher, B., Tirrell, D. A., and Finn, M. G. (2008) Unnatural amino acid incorporation into virus-like particles. *Bioconjugate Chem. 19*, 866–875.
40. van Hest, J. C. M., Kiick, K. L., and Tirrell, D. A. (2000) Efficient incorporation of unsaturated methionine analogues into proteins in vivo. *J. Am. Chem. Soc. 122*, 1282–1288.
41. Eriksson, A. E., Baase, W. A., Wozniak, J. A., and Matthews, B. W. (1992) A cavity-containing mutant of T4 lysozyme is stabilized by buried benzene. *Nature 355*, 371–373.
42. Eriksson, A. E., Baase, W. A., and Matthews, B. W. (1993) Similar hydrophobic replacements of Leu99 and Phe153 within the core of T4-lysozyme have different structural and thermodynamic consequences. *J. Mol. Biol. 229*, 747–769.
43. Ando, N., Barstow, B., Baase, W. A., Fields, A., Matthews, B. W., and Gruner, S. M. (2008) Structural and thermodynamic characterization of T4 lysozyme mutants and the contribution of internal cavities to pressure denaturation. *Biochemistry 47*, 11097–11109.
44. Kayser, B., Altman, J., and Beck, W. (1997) Alkyne bridged alpha-amino acids by palladium mediated coupling of alkynes with N-t-Boc-4-iodophenylalanine methyl ester. *Tetrahedron 53*, 2475–2484.
45. Hammill, J. T., Miyake-Stoner, S., Hazen, J. L., Jackson, J. C., and Mehl, R. A. (2007) Preparation of site-specifically labeled fluorinated proteins for ^{19}F-NMR structural characterization. *Nat. Prot. 2*, 2601–2607.

46. Mooers, B. H. M., and Matthews, B. W. (2004) Use of an ion-binding site to bypass the 1000-atom limit to structure determination by direct methods. *Acta Crystallogr., Sect. D 60*, 1726–1737.
47. Xie, J., and Schultz, P. G. (2005) An expanding genetic code. *Methods 36*, 227–238.
48. Xie, J., Liu, W., and Schultz, P. G. (2007) A genetically encoded bidentate, metal-binding amino acid. *Angew. Chem., Int. Ed. Engl. 46*, 9239–9242.
49. Neumann, H., Hazen, J. L., Weinstein, J., Mehl, R. A., and Chin, J. W. (2008) Genetically encoding protein oxidative damage. *J. Am. Chem. Soc. 130*, 4028–4033.
50. Pace, C. N. (1986) Determination and analysis of urea and guanidine hydrochloride denaturation curves. *Methods Enzymol. 131*, 266–280.
51. Lakowicz, J. R. (2006) Principles of Fluorescence Spectroscopy, 3rd ed., Springer Science and Business Media, LLC, New York.